Journal of Sound and Vibration (2002) **255**(3), 417–432
doi:10.1006/jsvi.2001.4163, available online at http://www.idealibrary.com on IDEAL®

THE INFLUENCE OF CONTROL SYSTEM DESIGN ON THE PERFORMANCE OF VIBRATORY GYROSCOPES

P. W. Loveday

Centre for Integrated Sensing Systems, CSIR, P.O. Box 395, *Pretoria* 0001, *South Africa*

AND

C. A. Rogers

College of Engineering, University of South Carolina, Columbia, SC 29208, *U.S.A.*

(*Received* 24 *May* 1999, *and in final form* 11 *June* 2001)

Understanding the influence of the control system on the performance of vibratory gyroscopes is important during the design of such devices. The ability of the control system to reduce the effects of resonator imperfections, on the gyroscope performance, was investigated. The analysis of the control problem presented begins with equations of motion describing the dynamics of a resonator including frequency and damping imperfections. These equations were transformed to slowly varying parameters and averaged. The equations of motion, in this form, provide many insights into the dynamics of the resonator and suggest the control system functions required to effectively operate the resonator as an angular rate sensor. A phase-locked loop-based control system was designed, analyzed and implemented. The control system drives the resonator at resonance to a constant amplitude and nulls the rotation-induced vibrations. It was shown analytically that the first order effects of frequency imperfections can be eliminated by the control system. The effect of damping anisotropy is not reduced by the control system and this is expected to be the major source of error in the closed-loop system. Experimental measurements, of a piezoelectrically actuated and sensed resonator, over a temperature range of 60°C, showed that variation of the zero-rate offset was decreased by an order of magnitude by the force-to-rebalance control. The analytical and experimental results present a convincing argument for the use of force-to-rebalance control in vibratory gyroscopes.

© 2002 Elsevier Science Ltd. All rights reserved.

1. INTRODUCTION

The advantages offered by vibratory gyroscopes have attracted a number of companies and researchers to this field. While one company has developed and produced the very high-performance hemisphere resonator gyro (HRG) [1, 2] the promise of low-cost, small and rugged sensors encouraged the development of several designs aimed at commercial applications. Recent efforts to develop micromachined designs were reviewed by Yazdi *et al.* [3].

The geometries used for the vibrating structure or resonator include hemispheres [1, 2] strings [4], beams [5, 6], tuning forks [7–9], rings [10–12], cylinders [13–15] and discs [16, 17]. These structures are excited and sensed by methods including electromagnetics, electrostatics and piezoelectricity.

Generally, one vibration mode of the resonator is excited at the resonant frequency. When the resonator is rotated, energy is coupled from this mode into a second vibration mode. This Coriolis coupling causes a response in the second vibration mode which is used

0022-460X/02/$35.00 © 2002 Elsevier Science Ltd. All rights reserved.

to measure the applied rotation rate. The response of this second mode is often controlled by a form of feedback control. This control is usually motivated by the need to increase the bandwidth of the gyroscope.

The performance of vibratory gyroscopes is limited by the effects of imperfections, in the resonator, which may be dependent on both time and temperature. The effects of imperfections in vibratory gyroscopes have been studied by various researchers [15, 18–21]. These studies focus on the effects of imperfections on the resonator dynamics and do not consider the design of the control system specifically to reduce the effects of imperfections. Numerous examples of micromachined vibratory gyroscope resonator developments are available in the literature [3]. Often the performance of these resonators is measured in simple open-loop tests which may not reflect the true potential of these devices. In this paper, the ability of the control system to suppress the effects of resonator imperfections is demonstrated analytically and experimentally.

The time-averaged equations of motion for a general resonator with mass/stiffness and damping imperfections are derived in the most natural form for analysis of angular rate sensor operation. The effects of imperfections may be understood qualitatively from these equations and the ability of control system functions to suppress the effects of certain imperfections is easily observed. Experimental results indicate the relative magnitude of imperfection effects which could be suppressed compared to those that could not be controlled, for a particular resonator.

2. MODEL OF RESONATOR DYNAMICS

The model of the resonator is required to describe the dynamics of the two modes of vibration and the Coriolis coupling between them. The resonators used are generally very lightly damped and the contribution of modes other than the operating modes is ignored.

2.1. EQUATIONS OF MOTION

The equations of motion of a "generic vibratory gyro" resonator are presented in equation (1). These equations describe the dynamics of an imperfect rotating axisymmetric shell resonator. Mass and stiffness imperfections cause a frequency difference between the two modes and also locate the modes relative to the shell. In the model the position of the lower frequency axis is specified and it is assumed that the two mode shapes are orthogonal. The damping of the resonator is described by two time constants representing an axis of minimum damping and an axis of maximum damping:

$$\begin{aligned}
&\ddot{x} - 2nk\Omega\dot{y} + (2/\tau + \Delta(1/\tau)\cos 2n\theta_\tau)\dot{x} + \Delta(1/\tau)\sin 2n\theta_\tau \dot{y} \\
&\quad + (\omega^2 - \omega\Delta\omega\cos 2n\theta_\omega)x - \omega\Delta\omega \sin 2n\theta_\omega y = f_x, \\
&\ddot{y} + 2nk\Omega\dot{x} + \Delta(1/\tau)\sin 2n\theta_\tau\dot{x} + (2/\tau - \Delta(1/\tau)\cos 2n\theta_\tau)\dot{y} \\
&\quad - \omega\Delta\omega \sin 2n\theta_\omega x + (\omega^2 + \omega\Delta\omega\cos 2n\theta_\omega)y = f_y.
\end{aligned} \tag{1}$$

Equation (1) is the same as that presented by Lynch [22] except that the factor n describing the number of circumferential waves has been included while the $\dot{\Omega}$ (angular acceleration) and Ω^2 (centrifugal acceleration) terms have been omitted.

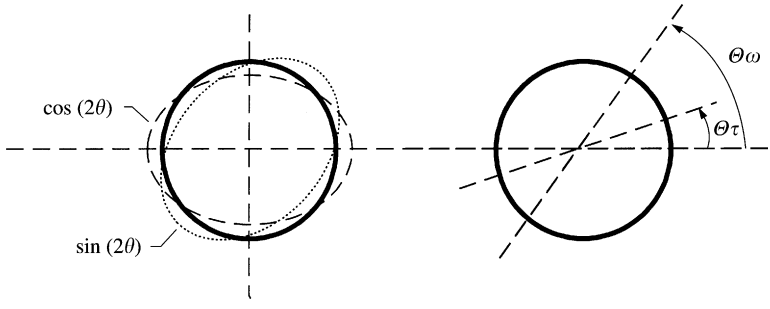

Figure 1. Vibration pattern representation and axis definitions.

The particular case of an axisymmetric shell resonator operating in the $n = 2$ modes is shown in Figure 1. Coriolis coupling between these two modes occurs when a rotation rate is applied around the axis of the resonator.

The equations of motion can be written in terms of the elements of a damping matrix and a "natural frequency" matrix to simplify the following manipulations. Equation (2) is applicable to resonators of other geometries which have two modes coupled by Coriolis effects:

$$\ddot{x} - g\Omega\dot{y} + c_{11}\dot{x} + c_{12}\dot{y} + k_{11}x + k_{12}y = f_x,$$

$$\ddot{y} + g\Omega\dot{x} + c_{21}\dot{x} + c_{22}\dot{y} + k_{21}x + k_{22}y = f_y. \tag{2}$$

2.2. AVERAGED EQUATIONS OF MOTION

Averaged equations of motion, describing the dynamics of a resonator including the effects of control loops, were derived by Lynch [22]. Use was made of "canonical" variables, which are invarient under rotation of the pickoff axis set around the axis of the resonator. These variables are necessary for describing the operation of the HRG as an angle sensor. These sophisticated equations may then be applied to the simpler case of an angular rate sensor with force-to-rebalance control. In this section, simple averaged equations of motion, for the resonator operating as an angular rate sensor are derived directly. The variables used in this analysis retain their physical meaning and provide good insight into the problem.

The dynamics of the resonator may be more efficiently described by transforming the system of two second order equations into a system of four first order equations in slowly varying parameters. The following transformation was used to transform the equations in the rapidly varying parameters, x and y into equations in the slowly varying parameters, X_s, X_c, Y_s and Y_c:

$$x = X_s \sin \nu t + X_c \cos \nu t, \qquad y = Y_s \sin \nu t + Y_c \cos \nu t. \tag{3}$$

After the manipulations and averaging, described in Appendix A, a system of four first-order equations in the slowly varying parameters is obtained. It was assumed that the resonator is lightly damped and has only small frequency and damping imperfections. The assumption is valid for resonators designed with two modes of vibration having nominally

the same frequency:

$$\dot{X}_s = -\frac{c_{11}}{2}X_s - \frac{(k_{11}-v^2)}{2v}X_c - \frac{(c_{12}-g\Omega)}{2}Y_s - \frac{k_{12}}{2v}Y_c + \frac{F_{x_c}}{2v},$$

$$\dot{X}_c = \frac{(k_{11}-v^2)}{2v}X_s - \frac{c_{11}}{2}X_c + \frac{k_{12}}{2v}Y_s - \frac{(c_{12}-g\Omega)}{2}Y_c - \frac{F_{x_s}}{2v},$$

$$\dot{Y}_s = -\frac{(c_{21}+g\Omega)}{2}X_s - \frac{k_{21}}{2v}X_c - \frac{c_{22}}{2}Y_s - \frac{(k_{22}-v^2)}{2v}Y_c + \frac{F_{y_c}}{2v},$$

$$\dot{Y}_c = \frac{k_{21}}{2v}X_s - \frac{(c_{21}+g\Omega)}{2}X_c + \frac{(k_{22}-v^2)}{2v}Y_s - \frac{c_{22}}{2}Y_c - \frac{F_{y_s}}{2v}. \tag{4}$$

In the averaging process a first-order approximation was made when it was assumed that the slowly varying parameters could be considered constant over one period of oscillation [23].

The form of this system of equations appears similar to state-space equations but these equations include frequency and the frequency-squared terms which are not present in a state-space system. This means that state-space methods of analyzing and designing control systems cannot be applied to this system. During operation the resonator is forced to vibrate at resonance at a constant amplitude. This limit cycle can only exist in a non-linear system which makes analysis of the control system difficult. Because the averaged equations above are in the slowly varying parameters it is possible to use time integration to simulate the operation of the closed-loop system. The averaged equations also provide some useful insights into the behaviour of the resonator which aid in the control system design.

3. CONTROL SYSTEM FUNCTIONS

In this section, the averaged equations of motion are used to motivate the control system functions required for the resonator to operate as an angular rate sensor. The equations of motion without imperfections are used to develop the control functions and the implementation of these functions. The effects of resonator imperfections, on the performance of the controlled system, are then analyzed in section 4.

The averaged equations of motion are simplified by the omission of imperfections:

$$\dot{X}_s = -(c/2)X_s - ((k-v^2)/2v)X_c + (g\Omega/2)Y_s + F_{x_c}/2v,$$

$$\dot{X}_c = ((k-v^2)/2v)X_s - (c/2)X_c + (g\Omega/2)Y_c - F_{x_s}/2v,$$

$$\dot{Y}_s = -(g\Omega/2)X_s - (c/2)Y_s - ((k-v^2)/2v)Y_c + F_{y_c}/2v,$$

$$\dot{Y}_c = -(g\Omega/2)X_c + ((k-v^2)/2v)Y_s - (c/2)Y_c - F_{y_s}/2v. \tag{5}$$

It is evident that in the perfect resonator the x and y vibration patterns are only coupled when an angular rotation rate (Ω) is applied. One makes use of this effect when using the resonator as an angular rotation sensor or gyroscope. In the ideal case, the control functions may be separated into those operating on the primary vibration pattern and those operating on the secondary vibration pattern.

3.1. CONTROL OF THE PRIMARY VIBRATION PATTERN

The equations of motion for the primary vibration pattern, in the absence of applied rotation rate are

$$\dot{X}_s = -\frac{c}{2} X_s - \frac{(k - v^2)}{2v} X_c + \frac{F_{x_c}}{2v}, \qquad \dot{X}_c = \frac{(k - v^2)}{2v} X_s - \frac{c}{2} X_c - \frac{F_{x_s}}{2v}. \tag{6}$$

The steady state response of the system is found by setting the time derivative terms to zero.

3.1.1. *Frequency control*

If one applies a sinusoidal excitation $f_x = \sin vt$ ($F_{xs} = 1$ and $F_{xc} = 0$) at the frequency $v = \sqrt{k_{11}}$, then the coupling between X_c and X_s is zero and the response will be $X_c = -F_{x_s}/vc_{11}$, $X_s = 0$. In other words, if one excites the structure at resonance the response will be 90° out of phase with the excitation. At frequencies of excitation other than the resonant frequency the equations are coupled and there will be sine and cosine response components. The damping, c, determines the amplitude of response at steady state and also the speed with which this amplitude changes. Note that in the first-order approximation the presence of damping does not affect the resonant frequency. Neglecting this second-order effect is justified because vibratory gyroscope resonators are designed to have very small damping.

The observation that there is a sine component response to a sine excitation if the excitation frequency does not coincide with the resonant frequency of the resonator suggests a method of controlling the frequency of excitation to follow the resonant frequency of the resonator. The sine component of the response (X_s) can be used as the error signal in a phase-locked loop which drives the resonator at resonance. This phase-locked loop consists of a sine-wave generator or voltage-controlled oscillator (VCO) which produces a sine wave, the frequency of which is determined by the voltage applied to the VCO. The sine wave is applied to the resonator and the response of the resonator is demodulated by the excitation sine to produce the amplitudes of the components which are in-phase (X_s) and in-phase quadrature (X_c) to the excitation signal. This demodulation can be achieved by a lock-in amplifier (LIA) which is a laboratory instrument specifically designed for this task. The response component X_s which is in-phase with the excitation is used as an error signal which is filtered by a proportional–integral controller before being fed back to control the frequency of the excitation signal generated by the VCO. This control loop is illustrated in Figure 2.

3.1.2. *Amplitude control*

The amplitude of response of the primary vibration pattern, when excited at resonance, is determined by the amplitude of the excitation and the damping in the resonator. The Coriolis forces experienced by the secondary vibration pattern are proportional to the product of the velocity of vibration of the primary vibration pattern and the applied rotation rate. The second function of the control system is to maintain the amplitude of the vibration of the primary mode at a constant value. Because the frequency control loop ensures that X_s is zero, the amplitude of the primary mode is given by X_c which is available from the lock-in amplifier used in the frequency control loop. The difference between the actual amplitude of vibration and a set reference value forms the error signal. Once again a proportional–integral controller is used to ensure that the steady state error is zero. The output from the proportional–integral controller is multiplied by the excitation signal from

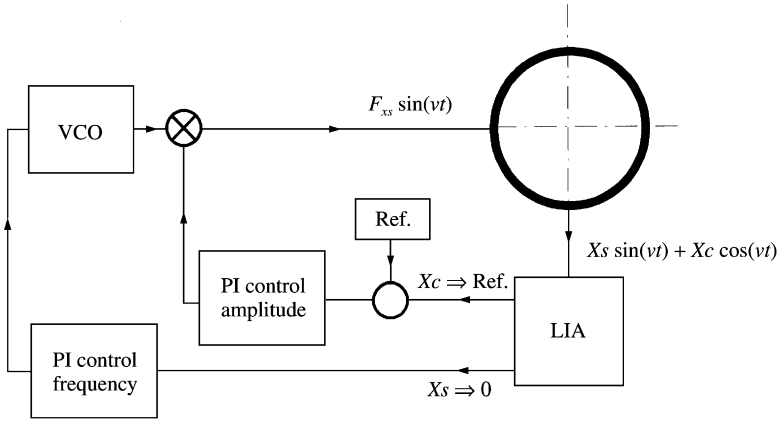

Figure 2. Frequency and amplitude control of primary vibration pattern by the phase-locked loop approach.

the VCO to control the amplitude of the signal applied to excite the resonator and thus the amplitude of the response of the resonator. The amplitude control loop is shown in Figure 2.

3.2. CONTROL OF THE SECONDARY VIBRATION PATTERN

If one assumes that the primary vibration pattern is excited to vibrate at resonance with constant amplitude ($X_s = 0$, $X_c = \bar{X}_c$) inspection of equation (5) shows that there will be a cosine response (Y_c) in the secondary vibration pattern when a constant rotation rate is applied. The response of the secondary vibration pattern to a step input angular rotation rate is easily calculated:

$$Y_{c_{step}} = -(g\Omega\bar{X}_c/c)(1 - e^{-(c/2)t}). \tag{7}$$

This open-loop response of the secondary vibration pattern gives the steady state amplitude which determines the scale factor of the gyroscope and also provides a measure of the response time. The open-loop bandwidth of typical resonators is usually too small for most applications. The effective damping of the resonator (c) can be increased electronically by applying velocity feedback [24]. It is also possible to null the response of the secondary vibration pattern by applying a suitable force F_{ys}. The control system used to supply this force will then determine the response time or bandwidth of the gyroscope. This method of control is known as force-to-rebalance because a force is applied which effectively balances the Coriolis force acting on the secondary vibration pattern. The rotation rate information is stored in the signal (F_{ys}) required to null the response. In this scheme, the secondary mode is not allowed to respond and the Coriolis forces experienced by the secondary mode are balanced by the control force F_{ys}. This is true closed-loop operation.

When imperfections are present there will be a sine response in the secondary vibration pattern (Y_s). Nulling the secondary vibration pattern requires that this component is also nulled. This case will be considered in order to investigate later the effects of imperfections on the gyroscope performance. The forces F_{ys} and F_{yc} required to null Y_c and Y_s, respectively, can be formed by two proportional–integral control systems as

$$F_{y_c} = -\left(K_P Y_s + K_I \int_0^t Y_c \, dt\right), \qquad F_{y_s} = K_p Y_c + K_I \int_0^t Y_c \, dt. \tag{8}$$

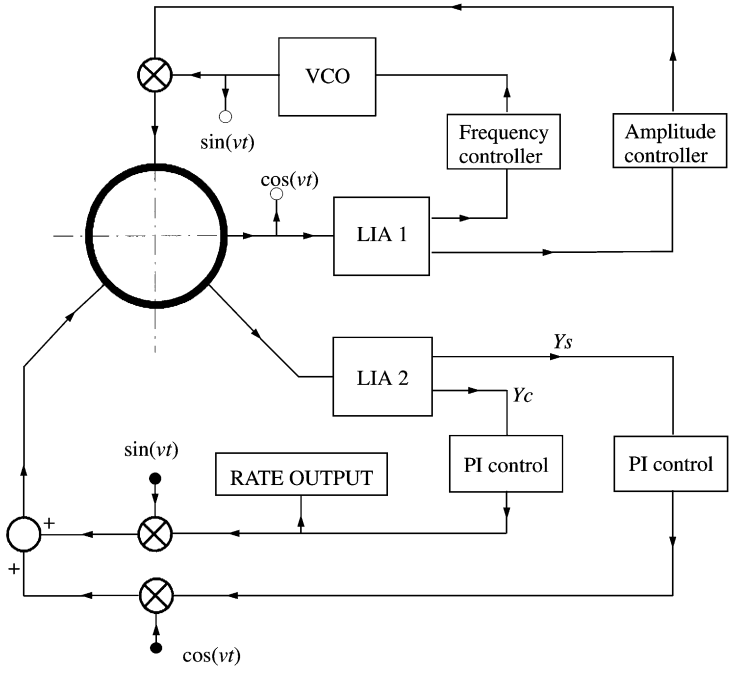

Figure 3. Force-to-rebalance control loop implementation shown with the primary vibration pattern control loops.

It is noted that if only the proportional part of the controller is applied one is essentially adding damping to the resonator. This would improve the bandwidth of the resonator at the cost of a degraded signal-to-noise ratio. The use of FTR means that the Coriolis forces acting on the secondary mode are balanced by the control forces and the position of the standing wave pattern is maintained fixed relative to the resonator. The choice of feedback control coefficients determines the speed of response of the closed-loop system and hence the bandwidth of the gyroscope. As there is no displacement or velocity of the secondary mode, changes in the damping factor, c_{22}, will also have no influence on the output. The damping anisotropy, c_{12}, will still have an effect on the output of the gyroscope and this will be the major source of error in the closed-loop system. This implementation of a force-to-rebalance control system is illustrated in Figure 3.

4. EFFECTS OF IMPERFECTIONS

In section 3, the control system functions were described for a perfect resonator. In this section, the effects of imperfections are analyzed qualitatively, by inspection of the averaged equations of motion, and quantitatively, by numerical solution of the non-linear equations. The effects of frequency and damping imperfections on the open-loop performance are determined. The ability of force-to-rebalance control to decrease this sensitivity to resonator imperfections is then considered.

In certain cases it is possible to calculate the steady state response of the controlled system but in general it was necessary to solve the non-linear equations numerically. The control functions were expressed mathematically as different sets of conditions depending on the control functions being analyzed. For the primary mode this implies that $F_{x_c} = 0$;

TABLE 1

Conditions used during steady state solutions

Primary mode conditions		Secondary mode control	Secondary mode parameters	
Set	Calculate		Set	Calculate
$F_{x_c} = 0$	v	Open loop	$F_{y_c} = F_{y_s} = 0$	Y_s, Y_c
$X_s = 0$	F_{x_s}			
$X_c = \bar{X}_c$	—	FTR	$Y_c = Y_s = 0$	F_{y_s}, F_{y_c}

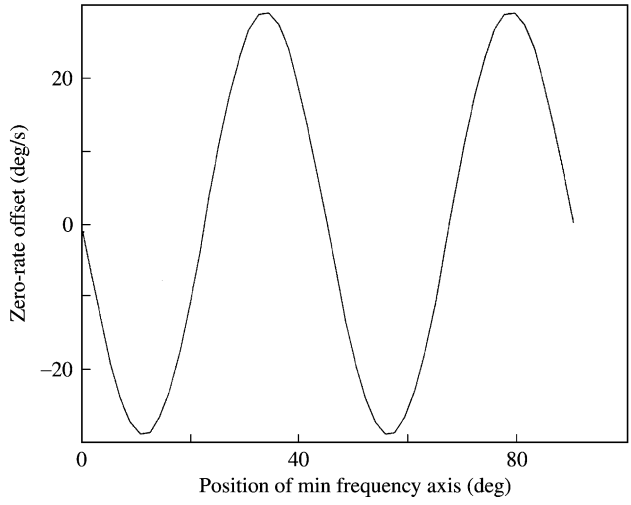

Figure 4. Zero-rate offset of a 15 kHz resonator with a 1 Hz frequency imperfection—open loop.

$X_s = 0$; $X_c = \bar{X}_c$ and the operating frequency, v, and the required drive amplitude, F_{xs} is calculated. The conditions applied to the secondary mode depend on the control loop selected. The prescribed conditions and the parameters which were calculated in each case are listed in Table 1.

4.1. OPEN-LOOP OPERATION

4.1.1. *Frequency imperfections*

The effect of frequency split (mass/stiffness anisotropy) was investigated. Equation (4) shows that elastic imperfections result in coupling between X_c and Y_s through k_{21} and then between Y_s and Y_c because $k_{22} \neq v^2$. The resulting response of Y_s and Y_c also couples back to the equations for X_s and X_c. Therefore, elastic anisotropy results in a complex coupling between all four of the averaged equations of motion. The output of the gyroscope will therefore be sensitive to variations in the elasticity of the resonator. A resonator with natural frequencies of 15 000 and 15 001 Hz was simulated with the angular position of the lower frequency mode varied between 0 and 90°. The scale factor of the gyroscope was determined by including a rotation rate in the model and calculating the resultant Y_c. The zero-rate drift, Y_c, due to the frequency imperfection, was then converted to a rotation rate in °/s and plotted in Figure 4.

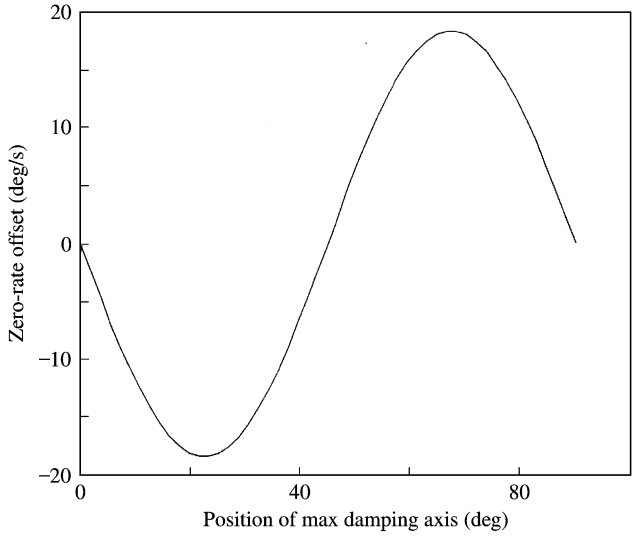

Figure 5. Zero-rate offset of a 15 kHz resonator with a damping imperfection defined by two time constants of $\frac{1}{25}$ and $\frac{1}{25.5}$ s—open loop.

4.1.2. *Damping imperfections*

If one considers damping anisotropy it can be seen that the terms $c_{12} = c_{21}$ appear with the Coriolis coupling terms. Therefore, if the primary mode is excited so that X_c is constant, the term c_{21} causes a response in Y_c which appears as an applied rotation rate. This means that there will be a zero-rate offset that will be sensitive to changes in the damping distribution of the resonator. The zero-rate offset and response to a step input angular rate are now

$$Y_c(\Omega = 0) = -(c_{21}/c_{22})X_c, \qquad Y_{c_{step}} = -((c_{21} + g\Omega)X_c/c_{22})(1 - e^{-(c_{22}/2)t}). \tag{9}$$

The effect of damping imperfections were investigated by introducing two damping time constants of $\frac{1}{25}$ and $\frac{1}{25.5}$ s (resonator Q-factor approximately 2000). The maximum damping axis was rotated and the zero-rate offset calculated for the open-loop case. The zero-rate offset is shown in Figure 5.

4.1.3. *Combined frequency and damping imperfections*

Finally, the effect of combined elastic and damping imperfections was considered. The zero-rate offset, due to elastic and damping imperfections acting simultaneously, was calculated by solving the steady state equations for different combinations of damping axis angle and frequency axis angle. This result is plotted as a surface in Figure 6. The drift obtained by adding the drifts calculated when the imperfections act independently was calculated and was found to be a good approximation of the drift due to the imperfections acting simultaneously. Also plotted in Figure 6 is the error caused by this approximation. This error can be written symbolically as

$$\text{ERROR}(\theta_\tau, \theta_\omega) = \text{Drift}(\theta_\tau, \theta_\omega) - (\text{Drift}(\theta_\tau) + \text{Drift}(\theta_\omega)).$$

The effects of the small frequency and damping imperfections considered here are therefore almost independent of each other.

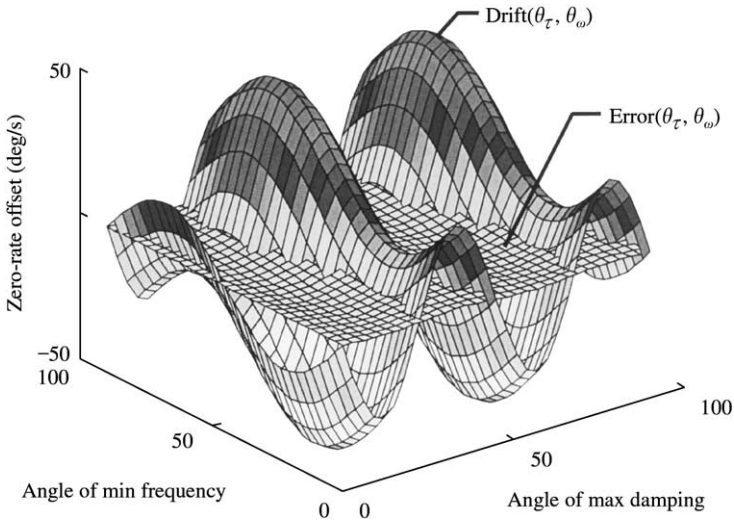

Figure 6. Zero-rate offset due to the combined effects of frequency and damping imperfections—open loop.

4.2. FORCE-TO-REBALANCE CONTROL

The effect of nulling the in-phase and quadrature components of the response separately and then simultaneously was considered to gain deeper insight into the effects of FTR control. The same imperfections as were considered in the open-loop case were included.

4.2.1. *Frequency imperfections*

Inspection of the averaged equations shows that frequency imperfections affect the output of Y_c only if Y_s is non-zero. Y_s is non-zero due to the term k_{21} coupling Y_s to X_c. Also, if Y_c is non-zero it couples back to the equation for X_s and thus influences the frequency of operation. It is therefore advantageous to null the component Y_s to eliminate this coupling.

Figure 7 shows that nulling the in-phase component eliminated the zero-rate offset caused by elastic imperfections, thus verifying the qualitative explanation given above. When only the quadrature component is nulled the zero-rate offset is not reduced from the open-loop case. The reason for nulling the quadrature component is to increase the bandwidth of the gyroscope.

4.2.2. *Damping imperfections*

The effect of damping imperfections was calculated in an analogous manner. The result showed that force-to-rebalance control does not reduce the drift caused by damping imperfections as represented in this analysis. Inspection of equation (4) shows that the damping imperfection is indistinguishable from an applied rotation.

5. EXPERIMENTAL INVESTIGATION

The total stiffness and damping of a resonator, and the distribution thereof, will vary with temperature. These temperature-dependent imperfections will result in an undesirable temperature-dependent zero-rate offset (gyroscope output with zero rotation rate). It was shown in section 4 that force-to-rebalance control suppresses the first order effects of

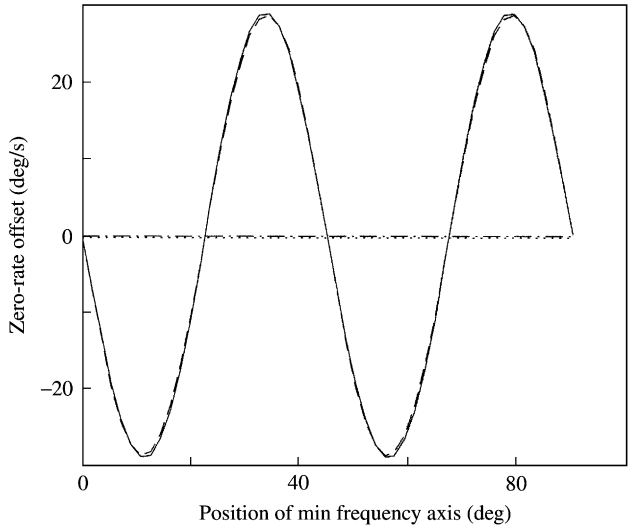

Figure 7. Suppression of the zero-rate offset due to frequency imperfections by FTR control: ——, open loop; – – –, only quadrature component nulled; – · – · –, only in-phase component nulled; · · · · ·, force-to-rebalance control.

stiffness distribution variation but not the effect of damping distribution variations. The relative contributions of these two imperfections is dependent on the particular resonator and this relative contribution was investigated experimentally for a piezoelectrically sensed and actuated vibrating cylinder resonator. Force-to-rebalance control was implemented and the results were compared to measurements with open-loop control.

5.1. EXPERIMENTAL SET-UP

The resonator used in the experiments comprised a thin-walled, steel cylinder, closed at one end, with eight discrete piezoelectric ceramic elements bonded near the open end [24]. Opposite pairs of ceramic elements were electrically connected and two pairs functioned as actuators while the remaining two pairs functioned as sensors. The resonator was enclosed in an evacuated housing to reduce acoustic radiation damping. The dynamics of the coupled electromechanical system have been reported previously [21].

The control systems described in section 3 were implemented using a combination of digital and analogue circuitry. In these experiments the control system was kept at room temperature while the resonator (with pre-amplifiers) was placed in an environmental chamber on a rate-table. The scale factor (mV/deg/s) of the gyroscope, with a particular control system, was measured at 20°C. The zero-rate offset of the gyroscope was then measured as a function of temperature over a range of 0–60°C, starting and finishing at 20°C. The measured voltage was converted to an equivalent rotation rate in deg/s using the measured scale factor. In this way it was possible to compare the variations in zero-rate offset of the gyroscope with the different control loops connected. All measurements were conducted on the same resonator.

5.2. EXPERIMENTAL RESULTS

Measurements were performed to investigate the effect of force-to-rebalance control on the temperature-induced zero-rate offset drift. The results of these measurements are shown

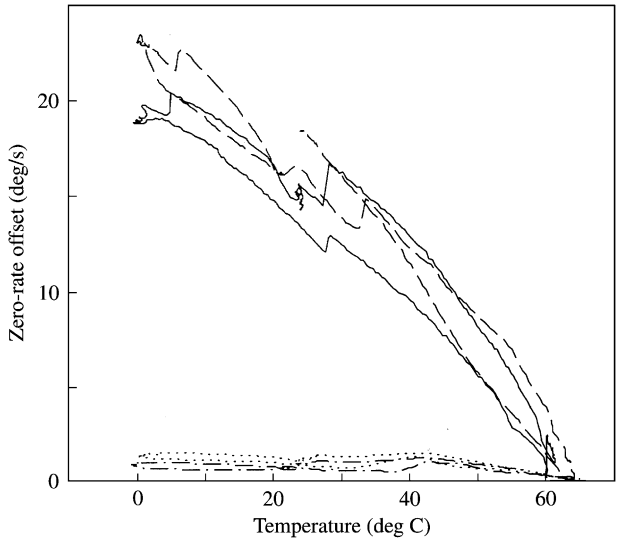

Figure 8. Measured reduction of temperature-induced zero-rate offset drift by FTR control: ——, open loop; – – –, only quadrature component nulled; – · – · –, only in-phase component nulled; · · · · ·, force-to-rebalance control.

in Figure 8. Apart from the control system in which both components of the secondary mode response were nulled, control systems where only one component was nulled were also examined. The results show a dramatic decrease in the drift when the in-phase component of the secondary mode is nulled. This result is in agreement with the theory as by nulling the in-phase component the effects of elastic imperfections are suppressed. It is evident that for the particular resonator the contribution of the temperature-dependent frequency imperfection was an order of magnitude larger than the effect of all other imperfections when operated with open-loop control. Force-to-rebalance control can therefore dramatically improve the performance of gyroscopes based on this type of resonator.

6. CONCLUSIONS

A system of averaged equations of motion describing the dynamics of a vibratory gyroscope resonator were presented. These equations are very convenient for analysis of control systems used to operate the resonator as a rotation rate sensor. The equations prompt the form of control system required and also provide useful insight into the qualitative effects of the resonator imperfections. Two control schemes were considered namely, open-loop control and force-to-rebalance control. The effects of frequency and damping imperfections were analyzed and it was shown that the force-to-rebalance control system can eliminate the first order effects of frequency imperfections. The effect of damping anisotropy is not reduced by the control systems and this is believed to be the major source of error in the closed-loop system. Experimental measurements, of a piezoelectrically actuated and sensed resonator, over a temperature range of 60°C, showed that variation of the zero-rate offset was decreased by an order of magnitude by the force-to-rebalance control. The remaining drift is believed to be primarily due to damping imperfections. The experimental results verified the theoretical predictions. It is clear that the performance of a resonator cannot be quantified from open-loop measurements alone.

ACKNOWLEDGMENTS

The first author wishes to acknowledge the useful discussions with Dr. M. Y. Shatalov and Dr. F. A. Koch during the course of this research and the assistance of Mr. H. Bothma and Mr. R. Sinclair during the construction of the resonators.

REFERENCES

1. E. J. Loper and D. D. Lynch 1983 *Proceedings of the IEEE/AIAA 5th Digital Avionics System Conference, Seattle, October* 1983. *Projected system performance based on recent HRG test results.*
2. *A. Matthews and F. J. Rybak* 1992 *IEEE AES Magazine* 1992. Comparison of hemispherical resonator gyro and optical gyros.
3. N. Yazdi, F. Ayazi and K. Najafi 1998 *Proceedings of the IEEE* **86**, 1640–1659. Micromachined inertial sensors.
4. W. H. Quick 1964 *Transactions of the ASME, Journal of Applied Mechanics* 523–534. Theory of the vibrating string as an angular motion sensor.
5. S. Fujishima, T. Nakamura and K. Fujimoto 1991 *Forty-fifth Annual Symposium on Frequency Control*, 261–265. Piezoelectric vibratory gyroscope using flexural vibration of a triangular bar.
6. H. Abe, T. Yoshida and K. Turuga 1992 *Japanese Journal of Applied Physics* **31**, 3061–3063. Piezoelectric-ceramic cylinder vibratory gyroscope.
7. G. H. Hunt and A. E. W. Hobbs 1965 *Symposium on Gyros, Proceedings of the Institution of Mechanical Engineers* (*London*) **179**, 129–139. Development of an accurate tuning-fork gyroscope.
8. W. S. Watson 1990 *IEEE Position Location and Navigation Symposium*, No. 90CH2811-8, 17–20. Vibrating element angular rate sensors for precision applications.
9. J. Söderkvist 1991 *IEEE Transactions on Ultrasonics, Ferroelectrics, and Frequency Control* **38**, 271–280. Piezoelectric beams and vibrating angular rate sensors.
10. J. C. Stiles 1975 U.S. Patent 3 926 475. Vibrating ring gyro.
11. M. W. Putty and K. Najafi 1994 *Solid-State Sensor and Actuator Workshop, Hilton Head, South Carolina*, 213–220. A micromachined vibrating ring gyroscope.
12. B. Johnson and I. M. Longden 1994 *Proceedings of the DGON Symposium on Gyro Technology, Stuttgart*. Vibrating structure gyroscopes and their applications.
13. R. M. Langdon 1982 *The Marconi Review* 231–249. The vibrating cylinder gyro.
14. J. S. Burdess 1986 *Proceedings of the Institution of Mechanical Engineers* **200**, 271–281. The dynamics of a thin piezoelectric cylinder gyroscope.
15. C. H. J. Fox 1988 *Proceedings of the DGON Symposium on Gyro Technology, Stuttgart*, chapter 5. Vibrating cylinder rate gyro: theory of operation and error analysis.
16. J. S. Burdess and T. Wren 1986 *IEEE Transactions on Aerospace and Electronic Systems* **AES-22**, 410–418. The theory of a piezoelectric disc gyroscope.
17. A. Jeanroy 1994 *Proceedings of the DGON Symposium on Gyro Technology*, Stuttgart, chapter 6. Low cost high dynamic vibratory rate gyro.
18. B. Friedland and M. F. Hutton 1978 *IEEE Transactions on Automatic Control* **AC-23**, 545–556. Theory and error analysis of vibrating-member gyroscope.
19. C. H. J. Fox 1994 *Proceedings of the DGON Symposium on Gyro Technology, Stuttgart*, chapter 5. Analysis and control of imperfection effects in vibratory gyros.
20. M. Y. Shatalov and P. W. Loveday 1995 *Proceedings of the DGON Symposium on Gyro Technology, Stuttgart*, chapter 15. A theory of errors in vibratory gyroscopes.
21. P. W. Loveday 1996 *Journal of Intelligent Material Systems and Structures* **7**(1), 44–53. A coupled electromechanical model of an imperfect piezoelectric vibrating cylinder gyroscope.
22. D. D. Lynch 1995 *Proceedings of the 2nd St. Petersburg International Conference on Gyroscopic Technology and Navigation, St. Petersburg, Russia*, 26–34. Vibratory gyro analysis by the method of averaging.
23. A. H. Nayfeh 1981 *Introduction to Perturbation Techniques*. New York: John Wiley & Sons, Inc.
24. P. W. Loveday and C. A. Rogers 1998 *IEEE Transactions on Ultrasonics, Ferroelectrics and Frequency Control* **45**, 1211–1215. Modification of piezoelectric vibratory gyroscope resonator parameters by feedback control.

APPENDIX A: DERIVATION OF AVERAGED EQUATIONS OF MOTION

A.1. VARIATION OF PARAMETERS

The equations of motion (equation (2)) in the rapidly varying parameters x and y,

$$\ddot{x} - g\Omega\dot{y} + c_{11}\dot{x} + c_{12}\dot{y} + k_{11}x + k_{12}y = f_x,$$

$$\ddot{y} + g\Omega\dot{x} + c_{21}\dot{x} + c_{22}\dot{y} + k_{21}x + k_{22}y = f_y, \tag{A1}$$

may be transformed into equations in slowly varying parameters X_s, X_c, Y_s and Y_c by the transformation (equation (3))

$$x = X_s \sin \nu t + X_c \cos \nu t, \qquad y = Y_s \sin \nu t + Y_c \cos \nu t. \tag{A2}$$

Differentiation of these two transformation equations yields

$$\dot{x} = \nu(X_s \cos \nu t - X_c \sin \nu t) + \dot{X}_s \sin \nu t + \dot{X}_c \cos \nu t,$$

$$\dot{y} = \nu(Y_s \cos \nu t - Y_c \sin \nu t) + \dot{Y}_s \sin \nu t + \dot{Y}_c \cos \nu t. \tag{A3}$$

Because the equations have been transformed from two parameters to four parameters one can introduce two restrictions in the new parameters [23]. The following choice of restrictions is very advantageous:

$$\dot{X}_s \sin \nu t + \dot{X}_c \cos \nu t = 0, \qquad \dot{Y}_s \sin \nu t + \dot{Y}_c \cos \nu t = 0. \tag{A4}$$

With these restrictions the velocities and accelerations become

$$\dot{x} = \nu(X_s \cos \nu t - X_c \sin \nu t), \qquad \dot{y} = \nu(Y_s \cos \nu t - Y_c \sin \nu t); \tag{A5}$$

$$\ddot{x} = -\nu^2(X_s \sin \nu t + X_c \cos \nu t) + \nu(\dot{X}_s \cos \nu t - \dot{X}_c \sin \nu t),$$

$$\ddot{y} = -\nu^2(Y_s \sin \nu t + Y_c \cos \nu t) + \nu(\dot{Y}_s \cos \nu t - \dot{Y}_c \sin \nu t). \tag{A6}$$

The velocities and accelerations are substituted into the equations of motion to yield

$$(k_{11} - \nu^2)(X_s \sin \nu t + X_c \cos \nu t) + \nu(\dot{X}_s \cos \nu t - \dot{X}_c \sin \nu t)$$

$$+ (c_{12} - g\Omega)\nu(Y_s \cos \nu t - Y_c \sin \nu t) + c_{11}\nu(X_s \cos \nu t - X_c \sin \nu t)$$

$$+ k_{12}(Y_s \sin \nu t + Y_c \cos \nu t) = F_{x_s} \sin \nu t + F_{x_c} \cos \nu t,$$

$$(k_{22} - \nu^2)(Y_s \sin \nu t + Y_c \cos \nu t) + \nu(\dot{Y}_s \cos \nu t - \dot{Y}_c \sin \nu t)$$

$$+ (c_{21} + g\Omega)\nu(X_s \cos \nu t - X_c \sin \nu t) + c_{22}\nu(Y_s \cos \nu t - Y_c \sin \nu t)$$

$$+ k_{21}(X_s \sin \nu t + X_c \cos \nu t) = F_{y_s} \sin \nu t + F_{y_c} \cos \nu t. \tag{A7}$$

The next step is to combine these equations with the restrictions in order to get four equations each containing only one time-derivative term. The process is illustrated for the first equation.

Multiplication of the first equation of motion by $\cos vt/v$ and adding the first restriction multiplied by $\sin vt$ yields the equation

$$\dot{X}_s = -((k_{11} - v^2)/v)(X_s \sin vt \cos vt + X_c \cos^2 vt)$$
$$- (c_{12} - g\Omega)(Y_s \cos^2 vt - Y_c \sin vt \cos vt) - c_{11}(X_s \cos^2 vt - X_c \sin vt \cos vt)$$
$$- (k_{12}/v)(Y_s \sin vt \cos vt + Y_c \cos^2 vt) + (F_{x_s}/v) \sin vt \cos vt + (F_{x_c}/v) \cos^2 vt. \quad \text{(A8)}$$

Similar manipulations yield equations for $\dot{X}_c$, $\dot{Y}_s$ and $\dot{Y}_c$.

A.2. AVERAGING

Equation (A8) shows that if the resonator is lightly damped, has small imperfections and is subjected to small control forces, the rate of change of X_s ($\dot{X}_s$) will be small. The same conclusion can be drawn for $\dot{X}_c$, $\dot{Y}_s$ and $\dot{Y}_c$. One can therefore assume that X_s, X_c, Y_s and Y_c are constant over one period of oscillation. This permits one to average the equations over one period of oscillation by applying the expressions

$$\frac{1}{T}\int_0^T \sin vt \cos vt \, dt = 0, \qquad \frac{1}{T}\int_0^T \cos^2 vt \, dt = \frac{1}{T}\int_0^T \sin^2 vt \, dt = \frac{1}{2}. \quad \text{(A9)}$$

The resulting averaged equation is then

$$\dot{X}_s = -\frac{c_{11}}{2} X_s - \frac{(k_{11} - v^2)}{2v} X_c - \frac{(c_{12} - g\Omega)}{2} Y_s - \frac{k_{12}}{2v} Y_c + \frac{F_{x_c}}{2v}. \quad \text{(A10)}$$

A further three equations can be extracted in this manner giving the following system of four first-order equations describing the dynamics of the resonator in the slowly varying parameters:

$$\dot{X}_s = -\frac{c_{11}}{2} X_s - \frac{(k_{11} - v^2)}{2v} X_c - \frac{(c_{12} - g\Omega)}{2} Y_s - \frac{k_{12}}{2v} Y_c + \frac{F_{x_c}}{2v},$$

$$\dot{X}_c = \frac{(k_{11} - v^2)}{2v} X_s - \frac{c_{11}}{2} X_c + \frac{k_{12}}{2v} Y_s - \frac{(c_{12} - g\Omega)}{2} Y_c - \frac{F_{x_s}}{2v},$$

$$\dot{Y}_s = -\frac{(c_{21} + g\Omega)}{2} X_s - \frac{k_{21}}{2v} X_c - \frac{c_{22}}{2} Y_s - \frac{(k_{22} - v^2)}{2v} Y_c + \frac{F_{y_c}}{2v},$$

$$\dot{Y}_c = \frac{k_{21}}{2v} X_s - \frac{(c_{21} + g\Omega)}{2} X_c + \frac{(k_{22} - v^2)}{2v} Y_s - \frac{c_{22}}{2} Y_c - \frac{F_{y_s}}{2v}. \quad \text{(A11)}$$

APPENDIX B: NOMENCLATURE

c_{11}, c_{12}, c_{21}, c_{22}	elements in general damping matrix
f_x	force applied to the $\cos(2\theta)$ vibrating pattern
f_y	force applied to the $\sin(2\theta)$ vibrating pattern
F_{x_s}, F_{x_c}	sin and cosine components of force applied to $\cos(2\theta)$ vibration pattern
F_{y_s}, F_{y_c}	sin and cosine components of force applied to $\sin(2\theta)$ vibration pattern
g	Coriolis coupling terms

k_{11}, k_{12}, k_{21}, k_{22}	elements in "natural frequency" matrix
K_1, K_P	coefficients of integral and proportional control
n	number of circumferential waves
x	displacement of the $\cos(2\theta)$ vibrating pattern
X_s, X_c	sin and cosine components of x
y	displacement of the $\sin(2\theta)$ vibrating pattern
Y_s, Y_c	sin and cosine components of y
θ_τ	angle to the first principal damping axis
θ_ω	angle to the first natural mode
v	frequency of oscillation
τ_1, τ_2	two principal time constants
$1/\tau = \frac{1}{2}(1/\tau_1 + 1/\tau_2)$	
$\Delta(1/\tau) = \frac{1}{2}(1/\tau_1 - 1/\tau_2)$	
ω_1	first natural frequency
ω_2	second natural frequency
$\omega^2 = (\omega_1^2 + \omega_2^2)/2$	
$\omega\Delta\omega = (\omega_1^2 - \omega_2^2)/2$	
Ω	applied angular rotation rate